Acta Astronautica 81 (2012) 667–674

Contents lists available at SciVerse ScienceDirect

Acta Astronautica

journal homepage: www.elsevier.com/locate/actaastro

A thrust formula for an MPD thruster with applied-magnetic field

M. Coletti

The Tony Davies High Voltage Laboratory, EEE research group, ECS, University of Southampton, SO17 1BJ, Southampton, United Kingdom

ARTICLE INFO

Article history:
Received 23 October 2011
Received in revised form
2 May 2012
Accepted 11 August 2012
Available online 24 October 2012

Keywords:
MPD
applied magnetic field
thrust formula

ABSTRACT

In this paper a thrust formula for applied field MPD will be presented. The swirling velocity will be derived from the magnetic stress tensor and its conversion into axial energy into the magnetic nozzle will be analytically treated. The theoretical prediction of both swirling velocity and thrust will be compared to the measurements showing a reasonable agreement.

1. Introduction

LOW thrust propulsive systems have a very important role in the accomplishment of space missions. For these systems electric thrusters are more suitable than chemical thrusters thanks to their higher specific impulse. Among electric thrusters the MPD (Magnetoplasmadynamic) thruster is able to provide one of the highest thrust densities processing input powers ranging from tens of kilowatts to some megawatts. In many experimental works the application of an external magnetic field has been found to increases the MPD performances. The purpose of this work is to develop an analytical theory able to predict the thrust generated by an applied-field MPD thruster and to compare it with experimental data present in the literature to assess its validity.

2. Hypotheses

To derive an analytical thrust formula the following hypotheses will be used: the applied field is assumed to be purely axial inside the thruster (with the field lines diverging only outside it), the total current I, mass flow rate $\dot{m}$ and axial velocity v_{z0} at the exit section of the anode are assumed not to be significantly influenced by the application of the magnetic field and the gas-dynamic thrust will be neglected in comparison with the electromagnetic one. The MPD thrust with no external-applied field can be then expressed as [1,2]

$$F_{B=0} = \frac{\mu I^2}{4\pi}\left[\ln\left(\frac{r_a}{r_c}\right) + \frac{3}{4}\right] \tag{1}$$

3. Effect of the applied magnetic field inside the MPD thruster

The main effect of the application of an axial magnetic field is the production of a swirling motion in the plasma jet [2–8] inside the MPD. Thanks to the effect of the magnetic nozzle created by the diverging magnetic field lines outside of the MPD the kinetic energy relative to the swirling velocity is transferred to the axial motion [7,9] hence increasing the MPD thrust.

To derive the swirling velocity the magnetic stress tensor will be used. The electromagnetic forces acting on the plasma can be expressed as [2]

$$\vec{F} = \int_V \vec{f}\, dV = \int_V \vec{j} \times \vec{B}\, dV \tag{2}$$

using Maxwell's equation $\nabla \times \vec{B} = \mu \vec{j}$ Eq. (2) becomes

$$\vec{f} = \vec{j} \times \vec{B} = \frac{1}{\mu}(\nabla \times \vec{B}) \times \vec{B} \tag{3}$$

E-mail address: coletti@soton.ac.uk

0094-5765/$ - see front matter © 2012 Elsevier Ltd. All rights reserved.
http://dx.doi.org/10.1016/j.actaastro.2012.08.014

Nomenclature

A	area
B	magnetic field
$\mathbf{B}$	magnetic stress tensor
F	force
f	force per unit volume
I	current
I_{in}	moment of inertia of the plasma column
I_m	current in the magnetic coil
j	current density
k	detachment parameter
m	mass of the plasma column inside the thruster
m_i	ionic mass
$\dot{m}$	mass flow rate
M	torque
n	normal
q	electron charge
R_m	magnetic coil radius
r	radius
S	surface
V	volume
v	velocity
v_{z0}	axial velocity at the exit of the thruster due to self field acceleration
z,θ,r	cylindrical coordinate
β	kinetic to magnetic energy ratio
θ_{div}	jet divergence angle
ρ	density
ω	angular velocity
μ	vacuum magnetic permeability
τ	residence time of the plasma inside the thruster

Subscript

a	relative to the anode or Alfven (in case of velocity)
B	relative to the magnetic field
$B=0$	without applied field
c	relative to the cathode
meas	measured
f	at the end of the magnetic nozzle
L	Larmor
t	relative to the cylindrical surface of the anode
th	theoretical
z,θ,r	direction
0	on the exit surface of the anode
//	parallel to the magnetic field lines
$\perp$	perpendicular to magnetic field lines

Superscripts

$\rightarrow$	vector
$\hat{}$	unit vector
$\bar{x}$	x at the detachment point

introducing the magnetic stress tensor B

$$\frac{1}{\mu}(\nabla \times \vec{B}) \times \vec{B} = \nabla \cdot \mathbf{B} - \frac{1}{\mu}\vec{B}\ \nabla \cdot \vec{B} \tag{4}$$

and using Maxwell's equation $\nabla \cdot \vec{B} = 0$ and the divergence theorem an expression for the force can be derived as [2]

$$\vec{F} = \int_V \vec{j} \times \vec{B}\, dV = \int_V \nabla \cdot \mathbf{B}\, dV = \int_S \mathbf{B} \cdot \hat{n} dS \tag{5}$$

Using Eq. (5) the forces acting on plasma can be expressed as the flux of the tensor B through the boundary surface of the volume V representing the thruster. The control surface of an MPD with cylindrical geometry is reported in Fig. 1.

The magnetic stress tensor in cylindrical coordinates has the following expression [2]

$$\mathbf{B} = \frac{1}{\mu}\begin{bmatrix} B_r^2 - \frac{B^2}{2} & \frac{B_r B_\theta}{r} & B_r B_z \\ \frac{B_\theta B_r}{r} & \frac{B_\theta^2}{r^2} - \frac{B^2}{2r^2} & \frac{B_\theta B_z}{r} \\ B_z B_r & \frac{B_z B_\theta}{r} & B_z^2 - \frac{B^2}{2} \end{bmatrix} \tag{6}$$

Inside the MPD the only non-zero components of the magnetic field are B_θ (the self-induced magnetic field) and B_z (the externally applied magnetic field) hence the stress tensor becomes

$$\mathbf{B} = \frac{1}{\mu}\begin{bmatrix} -\frac{B_\theta^2}{2} - \frac{B_z^2}{2} & 0 & 0 \\ 0 & -\frac{B_\theta^2 + B_z^2}{2r^2} & \frac{B_\theta B_z}{r} \\ 0 & \frac{B_z B_\theta}{r} & \frac{B_z^2}{2} - \frac{B_\theta^2}{2} \end{bmatrix} \tag{7}$$

The swirling motion is the result of a force applied in the azimuthal direction. Using the simplifying assumption that the current is purely radial on the anode surface S_a

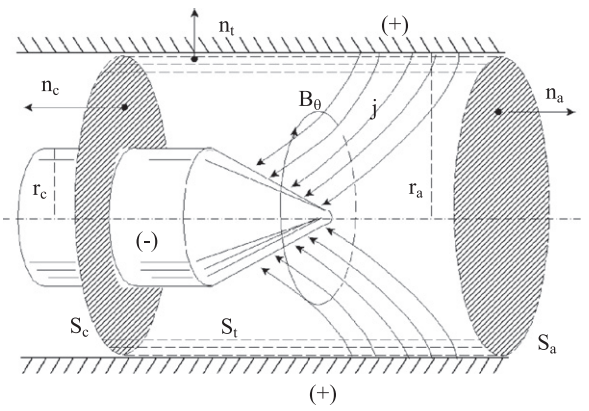

Fig. 1. Thruster geometry and integration surface [2].

and hence B_θ is zero on S_a, the only azimuthal force component is the one obtained from $\mathbf{B}\cdot\hat{n}_c$

$$F_\theta = \int_{S_c} \frac{B_\theta B_z}{\mu r}\, dS \tag{8}$$

Integrating Eq. (8)

$$F_\theta = B_z I\left(\ln\frac{r_a}{r_c}+\frac{1}{2}\right) \tag{9}$$

It can be noted that dimensionally F_θ is a force per unit length hence it will give rise to an angular acceleration. Assuming that the plasma rotates like a rigid body [5,10], the torque generated by F_θ can be expressed as

$$M = F_\theta \tilde{r}^2 = I_{\text{in}}\frac{\omega}{\tau} = m\tilde{r}^2\frac{\omega}{\tau} \tag{10}$$

where m represents the mass of the plasma column inside the thruster and $\tilde{r}$ is a mean value of the radius such that

$$I_{\text{in}} = \int_0^{r_a} \rho r^2 2\pi r dr = m\tilde{r}^2 \tag{11}$$

Noting that the mass flow rate is equal to $\dot{m} = m/\tau$ the angular velocity of plasma at the exit of the thruster can be expressed as

$$\omega = \frac{F_\theta}{\dot{m}} = \frac{B_z I}{\dot{m}}\left(\ln\frac{r_a}{r_c}+\frac{1}{2}\right) \tag{12}$$

The expression found for the angular frequency of the swirling motion is in formal agreement with those already derived by Mikellides [3], Fradkin [4] and Sasoh [10] showing a linear dependence from the "current times applied field" term and an inverse proportionality to the mass flow rate.

4. Effect of the applied magnetic field outside the MPD thruster: The magnetic nozzle

4.1. Transfer of kinetic energy from the swirling to the axial motion

Outside the MPD thruster the magnetic field lines diverge creating a magnetic nozzle. The effect of the magnetic nozzle is mainly to transfer the kinetic energy of a particle from its motion perpendicular to the magnetic field lines towards the direction parallel to the field [9]. In particular it can be demonstrated that the magnetic moment is conserved [11], hence taking two points along the trajectory of a particle (indicated with the subscripts 1 and 2, respectively) the relation between perpendicular velocity and magnetic field is [11]

$$\frac{v_{\perp 1}^2}{B_1} = \frac{v_{\perp 2}^2}{B_2} \tag{13}$$

Ideally this transfer lasts until the scale of the swirling motion perpendicular to the field lines is smaller than the scale of the variation of the field

$$\frac{\|\nabla\vec{B}\|}{B} r_L \ll 1 \tag{14}$$

To calculate the fraction of the kinetic energy that is transferred from the swirling to the axial motion (hence generating thrust) it is important to know where the particles "detach" from the magnetic nozzle, and so where the energy transfer ends. It will be assumed that the detachment happens when the ratio of the characteristic scales of the magnetic field and swirling motion reaches a critical value k.

$$\frac{\|\nabla\vec{B}\|}{B} r_L = k \tag{15}$$

It will also be assumed that the detachment happens far enough from the magnetic field source to consider it like a magnetic dipole. This assumption allows the expression of the magnetic field components and of the magnetic field strength as

$$B_r = \frac{\mu I_m R_m^2}{4}\frac{3zr}{(z^2+r^2)^{5/2}} \quad B_z = \frac{\mu I_m R_m^2}{4}\frac{2z^2-r^2}{(z^2+r^2)^{5/2}}$$
$$B = \frac{\mu I_m R_m^2}{4}\frac{\sqrt{4z^2+r^2}}{(z^2+r^2)^2} \tag{16}$$

Expressing $\|\nabla\vec{B}\|$ like $|\nabla\vec{B}\times\hat{B}|$, substituting into Eq. (15) and assuming that when a particle detaches from the magnetic field lines it is sufficiently near to the axis to neglect r^2 in comparison with z^2 the detachment point abscissa can be obtained as

$$\bar{z} = \left(R_m^{3/2}\frac{B_0}{3}\frac{q}{m_i}\frac{k}{v_{\perp 0}}\right)^2 = \frac{\alpha k^2}{v_{\perp 0}^2} \quad \alpha = \left(R_m^{3/2}\frac{B_0}{3}\frac{q}{m_i}\right)^2 \tag{17}$$

Now substituting Eq. (17) and the third of Eq. (16) into Eq. (13) and remembering that $\bar{z}^2 \gg \bar{r}^2$ the residual velocity perpendicular to field lines is

$$\bar{v}_\perp = v_{\perp 0}\sqrt{\frac{\bar{B}}{B_0}} = v_{\perp 0}^4\sqrt{\frac{R_m^3}{\alpha^3 k^6}} \tag{18}$$

Hence from the conservation of kinetic energy the velocity parallel to the magnetic field lines at the exit of the magnetic nozzle is

$$\bar{v}_{//} = \sqrt{v_0^2 - v_{\perp 0}^8\frac{R_m^3}{\alpha^3 k^6}} \tag{19}$$

According to [12] the detachment of the plasma from a magnetic nozzle happens when the velocity of the flow along the magnetic field lines equals the local Alfven velocity hence when $\beta=1$. The Alfven velocity at the detachment is $v_a = \bar{B}/\sqrt{\mu\bar{\rho}}$. From the conservation of mass the density at the detachment can be expressed as

$$\bar{\rho} = \rho_0\frac{v_{z0}}{v_a}\frac{A_0}{\bar{A}} \tag{20}$$

Considering the stream tube going from A_0 to $\bar{A}$ and imposing $\nabla\cdot B=0$ the ratio of the areas can be expressed as $A_0/\bar{A} = \bar{B}/B_0$. Using this relation in Eq. (20) the Alfven velocity at the detachment can be expressed as

$$v_a = \frac{\bar{B}}{\sqrt{\mu\rho_0\beta_0}} \tag{21}$$

substituting now Eq. (21) in Eq. (19) and using Eqs. (16) and (17) an expression for $\bar{z}$ can be derived

$$\frac{v_{a0}^2}{\beta_0}\left(\frac{R_m}{\bar{z}}\right)^6 + v_{\perp 0}^2\left(\frac{R_m}{\bar{z}}\right)^3 - v_0^2 = 0 \tag{22}$$

From the solution of Eq. (22) and Eq. (17) the value of k corresponding to the assumption that the detachment happens when the fluid reaches the Alfven speed can be derived; looking at Eq. (22) it can also be noted that k scales as $B_0^{1/3}$.

4.2. Divergence calculation

To calculate the axial component of the velocity derived in Eq. (19) the magnetic field divergence must be calculated. According to what reported in [13] the divergence can be expressed as

$$\beta(z) = \beta_0 \frac{z}{r_0} \tan^2 \theta_{\mathrm{div}} \sec^4 \theta_{\mathrm{div}} \tag{23}$$

where $\beta(z)$ is the kinetic to magnetic energy ratio at a given abscissa z, β_0 is the value of β at the center of the current loop and r_0 is the radius of the plasma at $z=0$. Assuming again that the detachment happens when $\beta=1$, Eq. (23) can be expressed in terms of the cosine of the divergence angle as

$$\frac{r_0}{\beta_0 \bar{z}(k)} \cos^6 \theta_{\mathrm{div}} + \cos^2 \theta_{\mathrm{div}} - 1 = 0 \tag{24}$$

from which for every value of r_0 the value of θ_{div} can be calculated.

5. Thrust formula

From the expression of the velocity parallel to the magnetic field lines and of the divergence angle an effective value of the velocity can be expressed as

$$v_{z\,eff} = \frac{\int_A \overline{v}_{//} \cos\theta_{\mathrm{div}} dA}{\int_A dA} = \frac{\int_A \sqrt{v_{z0}^2 + \omega^2 r^2 - \omega^8 r^8 \frac{R_m^3}{\alpha^3 k^6}} \cos\theta_{\mathrm{div}} dA}{\int_A dA} \tag{25}$$

The integral in Eq. (25) has no analytical solution. To solve Eq. (25) the integrand will be interpolated with a polynomial. Considering that given Eq. (24) the dependency of $\cos\theta_{div}$ from r is quite weak the integrand can be generally expressed as $\sqrt{C^2 + D^2 r^2}$ where now r is normalized and hence varies from 0 to 1. Since in our case C and D are of comparable magnitude the integrand will have a parabolic trend for low values of r and a linear one for values of r close to 1 hence the integrand will be interpolated with a second order polynomial:

$$v_{z\,eff} = \frac{\int_0^{r_a} (ar^2 + b) r dr}{\int_0^{r_a} r dr} = \frac{1}{2} a r_a^2 + b \tag{26}$$

where the constants a and b can be determined imposing that the function (ar^2+b) is equal to the integrand of Eq. (25) at $r=0$ and $r=r_a$ obtaining

$$a = \frac{-v_{z0} + \sqrt{v_{z0}^2 + \omega^2 r_a^2 - \omega^8 r_a^8 \frac{R_m^3}{\alpha^3 k^6}} \cos\theta_{\mathrm{div}}}{r_a^2} \qquad b = v_{z0} \tag{27}$$

where in Eq. (27) $\cos\theta_{div}$ is calculated at $r_0 = r_a$. The thrust can be then calculated as

$$F_B = \frac{1}{2} \left(v_{z0} + \sqrt{v_{z0}^2 + \omega^2 r_a^2 - \omega^8 r_a^8 \frac{R_m^3}{\alpha^3 k^6}} \cos\theta_{\mathrm{div}} \right) \dot{m} \tag{28}$$

Noting that, as said before, k scales as $B_0^{1/3}$ and noting from Eq. (17) that α scales as B_0^2 it can be seen how for $B_0 \to 0$ Eq. (28) converges to a value of thrust that is lower than $F_{B=0}$ since the negative term under the square root tends to a finite value instead of vanishing. This is due to the assumption according to which the detachment happens far enough from the magnetic field source to consider it as a magnetic dipole; assumption that fails when the field tends to zero. For this reason in the calculation presented in the next sections when the thrust predicted from Eq. (28) drops below $F_{B=0}$ the value calculated with Eq. (1) will be used instead.

6. Comparison with experimental results

In this section a comparison between the theory developed above and experimental results is presented. First the comparison will focus on the angular velocity prediction and then will move to the propulsive characteristics (thrust and specific impulse) of existing thrusters.

6.1. Angular velocity

The angular velocity calculated from Eq. (12) will be compared to the measurements performed by Powers and Patrick [6] and by Tobari et al. [5]. In [6] an MPD with constant annular geometry has been investigated using four coils to produce a uniform magnetic field for a distance of 20 cm downstream of the discharge. The ratio of the swirling to axial velocity has been measured using a differential yaw probe. The results are plotted below together with the predictions obtained using Eq. (12)

In Fig. 2 the solid black line represent the v_θ/v_x ratio calculated in [6] using a momentum balance between the flow and the measured $j \times B$ forces. The dashed line is the ratio calculated including the shear stresses due to flow viscosity assuming a Reynolds number of 1000. The values of the v_θ/v_x ratio calculated using Eq. (12) are in close agreement with the prediction formulated in [6] for the inviscid case whereas the agreement with the experimental data is not as good showing an error of about 30%.

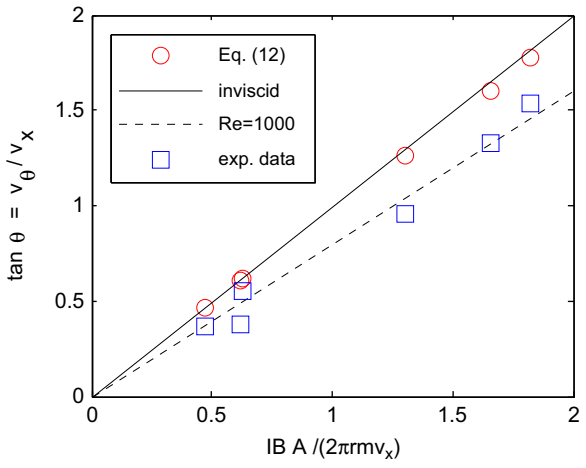

Fig. 2. Measured and predicted swirling to axial velocity ratios [6].

The difference between the predicted and experimental data is to be expected since viscosity is not taken into account in Eq. (12).

In [5] an MPD thruster has been operated with currents in the kilo-ampere range, applied fields up to 1000 G and using helium as a propellant. The azimuthal velocity has been measured using a spectroscopic method. The plasma has been found to rotate as a rigid body with a constant angular velocity [5] confirming the assumption made in Section 2. The azimuthal velocity measured at 1 cm from the thruster axis was 10 km/s at $I=7.2$ kA for a nominal applied field of 870 G. For this operating condition the actual magnetic field on the thruster axis was measured to be only 200 G at the location where the azimuthal velocity profile was measured (9 cm from the thruster exit). This was explained noting the very high ion temperature (of the order of 15 eV) and the consequent diamagnetic effect [5].

Using the measured value of the applied field the azimuthal velocity at 1 cm from the thruster axis calculated using Eq. (12) is 23 km/s hence overestimating the measurement by 130%. An explanation for this can be found in [5] where the different forces producing the swirling motion have been derived. In particular it has been shown how the diamagnetic drift has an opposite direction with respect to the $E\times B$ drift hence reducing the swirling velocity. Due to the very high value of the ion temperature the diamagnetic drift has been estimated to be 64% of the $E\times B$ drift [5]. Considering this the angular velocity induced by $E\times B$ relative to the measurements in [5] can be estimated to be 27.7 km/s. This value is in closer agreement with the 23 km/s estimate from Eq. (12) since the diamagnetic effect has not been taken into account in the derivation made in Section 3.

In conclusion from the comparison with the experimental data in [5,6] the formula derived for the calculation of the swirling angular velocity has been found to be able to reproduce the effect of the $E\times B$ drift within a 20% error. As expected the formula is not able to account for any viscous of diamagnetic effects hence caution must be used when the effects of these two phenomena are expected to significantly influence the swirling motion (very viscous fluids and/or very high temperature ions).

6.2. Propulsive performance

The comparison between the thrust predicted by Eq. (28) and the experimental data will be performed using the data reported in [14–19]. In most of the comparisons it has been found that if the value of k obtained from Eqs. (17) and (21) is increased by 10% the agreement between experimental and theoretical data is considerably improved. In particular it must be noted how to improve the agreement with the experimental data the value of k needed to be increased by 10%. The increase in k with respect to the value calculated from Eqs. (22) and (17) means that the detachment does not happens when the flow has reached the Alfven velocity ($\beta=1$) but when the ratio of the magnetic and swirling motion characteristic scale is 10% higher than the one relative to the position where $\beta=1$. This means that the detachment point is moved downstream allowing a bigger share of the kinetic energy relative to the swirling motion to be transferred to the axial motion hence producing higher values of thrust. In the comparisons reported below the results relative to both values of k will be presented.

6.2.1. Myers 100 kW MPD [14]

In Ref. [14] an experimental campaign has been carried out using different electrodes configurations and using a constant discharge current of 1000 A, a mass flow rate of 0.1 g/s of Argon and applied fields in the range 20–150 mT. The different geometries used are reported in Table 1.

As it has been anticipated before the agreement using the value of k from Eqs. (17) and (21) (dashed lines) is not good. The agreement is considerably improved increasing the value of k by 10% (solid lines). The theoretical data are well in agreement with the measurements for geometries B, C, E and G whereas the agreement is not as good for geometry H and non satisfactory for geometry A. Figs. 3–5.

6.2.2. MY-III thruster [15]

The MY-III thruster has been tested in [15] using two different configurations for the magnetic coil. The first one (CL1) is able to produce a magnetic field of 0.1 T on the axis of the thruster whereas the second one (C2L) produces a magnetic field of 0.21 T. The thruster has been run with 0.4 g/s of hydrogen.

Table 1
Mayer 100 kW thruster geometries [14]. Measurements in cm.

Geometry	Anode radius	Anode length	Cathode radius	Cathode length	Coil radius
A	2.5	7.6	0.64	7.6	7.65
B	3.81	7.6	0.64	7.6	7.65
C	5.1	7.6	0.64	7.6	10.15
D	5.1	15.2	0.64	7.6	10.15
E	5.1	7.6	1.27	7.6	10.15
F	5.1	15.2	1.27	7.6	10.15
G	3.81	7.6	0.64	2.5	7.65
H	2.5–5.1 (flared)	7.6	0.64	7.6	10.15

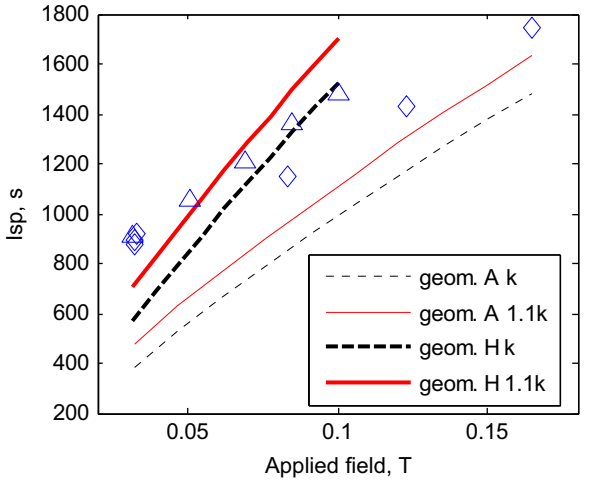

Fig. 3. Myers 100 kW. $\dot{m}=0.1$ g/s, I=1 kA. ◇ – geometry A, Δ – geometry H.

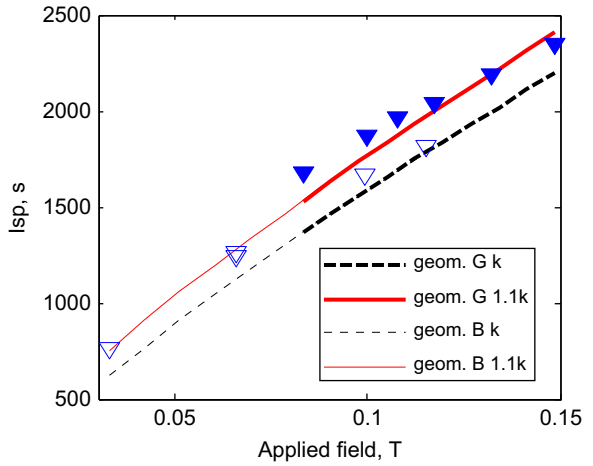

Fig. 4. Myers 100 kW. $\dot{m}=0.1$ g/s, $I=1$ kA. ▽ – geometry B, ▼ —geometry G.

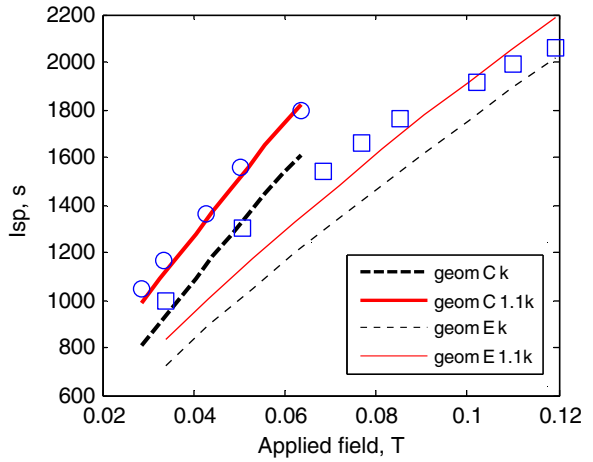

Fig. 5. Myers 100 kW. $\dot{m}=0.1$ g/s, $I=1$ kA. ○ – geometry C, □ – geometry E.

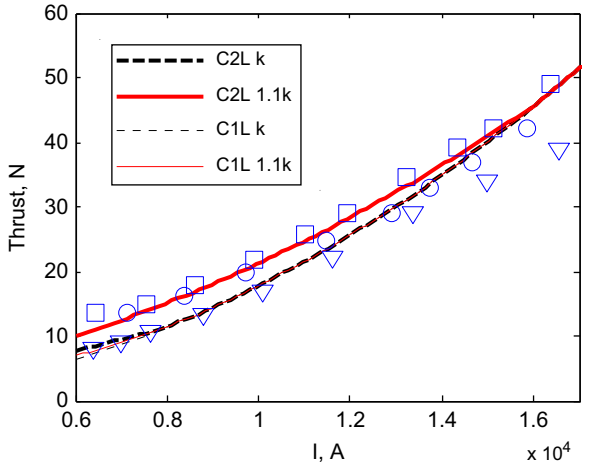

Fig. 6. MY-III. $\dot{m}=0.4$ g/s. ▽ – $B=0$, ○ – C1L configuration $B=0.1$ T, □ – C2L configuration $B=0.21$ T.

In the case of the C1L data in Fig. 6 the agreement between the theory and the data is poor with the theory basically predicting no improvements with respect to $B=0$ case (in fact the thin solid and dashed line are overlapping). The agreement is instead quite good for the C2L case when the augmented value of k is used.

6.2.3. *Tokyo 10 kW thruster [16]*

The Tokyo 10 kW thruster has a convergent divergent anode and has been tested in [16] using 30 mg/s of Argon, currents varying from 300 to 700 A and with applied fields in the range 0–4000 G.

In the simulation of the Tokyo 10 kW thruster no difference has been found between the calculations performed with the value of k from Eqs. (17) and (21) (dashed lines) and with the augmented k (solid lines). It can be seen from Fig. 7 and Fig. 8 how the calculated data exhibit the right trend but significantly underestimate the measurements. It must be noted that the theory underestimates the measurements even at $B=0$ (Eq. (1) is not

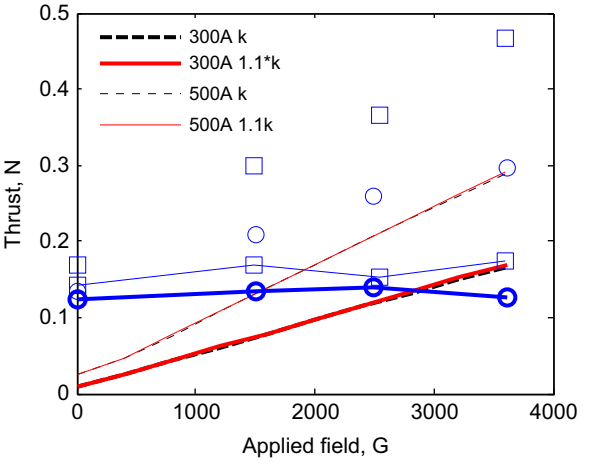

Fig. 7. Tokyo 10 kW. $\dot{m}=30$ mg/s. ○ – $I=300$ A, —○— – $F_{meas}-F_{th}$ $I=300$ A, □ – $I=500$ A, —□— – $F_{meas}-F_{th}$ $I=500$ A.

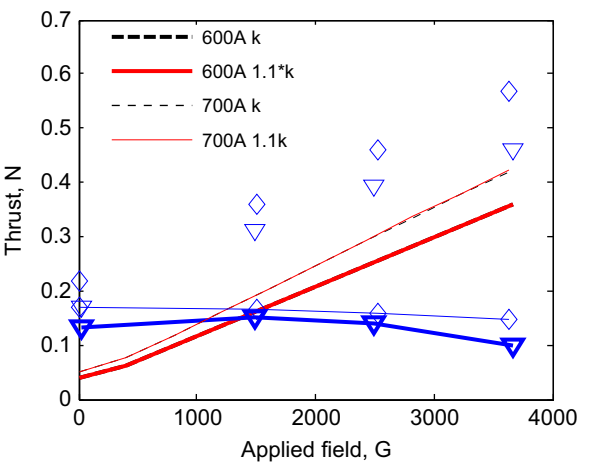

Fig. 8. Tokyo 10 kW. $\dot{m}=30$ mg/s. ▽—I=600 A, —▽— – $F_{meas}-F_{th}$ $I=700$ A, ◇ – $I=700$ A, —◇— $F_{meas}-F_{th}$ $I=700$ A.

able to predict the thrust produced with no applied magnetic field), from this it may be inferred that this is due to a significant gasdynamic contribution to the total thrust. The difference between the measured and predicted thrust has been plotted in every case (solid-marked lines in Fig. 8). As it can be seen from Figs. 7 and 8 this difference stays roughly constant with the applied magnetic field for each current level. It can be then concluded that in this case the theory is able to correctly represent the increase in electromagnetic thrust due to the magnetic field application but, as expected, cannot account for thermal effects.

6.2.4. MAI 130 kW thruster [17,18]

The MAI thruster has a convergent divergent anode and the magnetic coils are able to provide magnetic fields up to 0.13 T. In [17,18] it has been operated using Lithium as a propellant with mass flow rates in the range 0.45–0.95 mg/s, currents going from 1200 to about 2000 A and applied field values of 0.04 and 0.09 T.

As it can be seen in Fig. 9 the measured thrust depends on the mass flow rate (look for example at the $B=0.04$ T case). The theory has a very weak dependency on $\dot{m}$ and in this case the curves relative to different mass flow rates for the same level of applied field completely overlap, hence only one curve for every level of applied field has been reported. The agreement between the theoretical and experimental data this is good for the 0.09 T case whereas the predicted data underestimates the measurements at 0.04 T.

6.2.5. HPT Centrospazio [19]

The HPT is a coaxial thruster and in [19] it has been operated using Argon as a propellant with mass flow rates of 220 and 660 mg/s, currents in the range 1000–4000 A and applied field of 0.04 and 0.09 T.

In Fig. 10 the agreement between the experimental and theoretical data is reasonable when the augmented value of k is used. The numerical trends have found to be steeper than the experimental one with the numerical

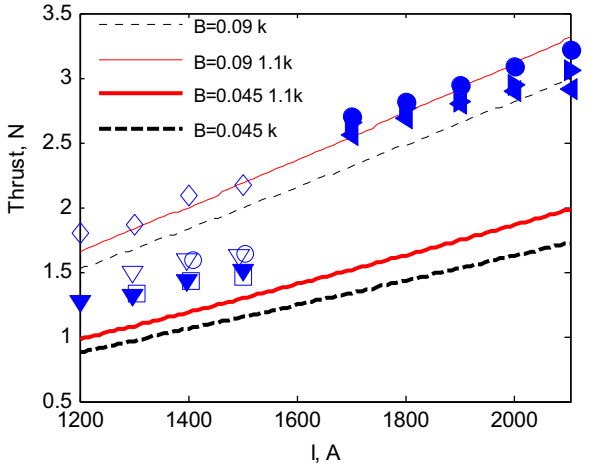

Fig. 9. MAI 130 kW. $B=0.045$ T □ – 0.45 mg/s, ▼ – 0.47 mg/s, ○ – 0.61 mg/s, ∇ – 0.62 mg/s. $B=0.09$ T ◇ – 0.65 mg/s, ◄ – 0.81 mg/s, ► – 0.86 mg/s, ● – 0.94 mg/s.

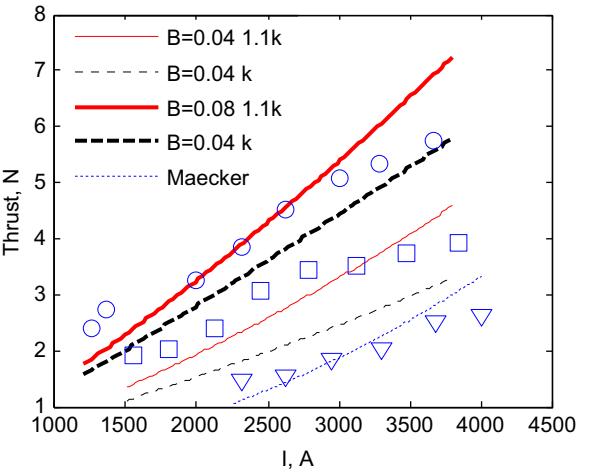

Fig. 10. HPT Centrospazio. $\dot{m}=220$ mg/s, ∇ – $B=0$, □ – $B=40$ mT, ○ – $B=80$ mT.

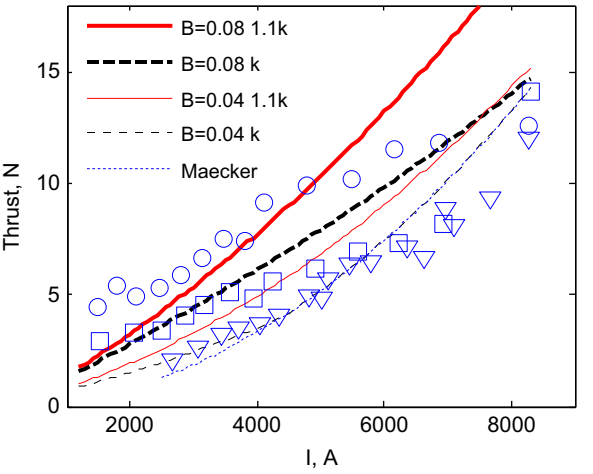

Fig. 11. HPT Centrospazio. $\dot{m}=660$ mg/s, ∇ – $B=0$, □ – $B=40$ mT, ○ – $B=80$ mT.

data overestimating the measurements at high current levels.

A similar situation is found in Fig. 11 where the trend of the numerical data is steeper than the experimental one overestimating measurements at high current levels. In this case the agreement is generally worse than in Fig. 10.

7. Conclusions

The theory developed in this paper has been compared with experimental results. Comparisons have been made both regarding the swirling angular velocity and the thrust/specific impulse produced by AF-MPD thrusters. The theory has been found to be able to represent the effect of the $E\times B$ drift on the swirling motion. The calculated value of the angular velocity are in qualitative agreement with the prediction derived in [6] for the inviscid case and tend to overestimate the measurements by 30%. The agreement is instead poor with the data

reported in [5] due to the strong diamagnetic effects present in that experiment. If the $E \times B$ contribution is extrapolated form the measurements according to what reported in [5] the agreement is improved with an error of about 20%.

Regarding the thrust predictions comparisons have been performed using data from 5 thrusters covering a current range from 300 to 20,000 A and a range of applied fields going from 0 to 0.4 T. The agreement has been found to be overall acceptable given the assumptions made in the theory development.

References

[1] H. Maecker, Plasmaströmungen in Lichtbögen infolge eigenmagnetischer Kompression, Z. Phys. 141 (1) (1955).
[2] R. Jahn, Physics of Electric Propulsion, McGraw-Hill, New York, 1968.
[3] P. Mikellides, P.J. Turchi., Applied-field magnetoplasmadynamic thrusters, Part 2: Analytic expressions for thrust and voltage, J. Propul. Power 16 (5) (2000).
[4] D.B. Fradkin. Analysis of Acceleration Mechanisms and Performance of an Applied Field MPD Arcjet. Ph.D. Dissertation, Princeton University MAE Department 1973.
[5] H. Tobari, A. Ando, M. Inutake, K. Hattori, Characteristics of electromagnetically accelerated plasma flow in an externally applied magnetic field, Phys. Plasmas 14 (2007).
[6] W.E. Powers, R.M. Patrick, Magnetic annular arc, Phys. Fluids 10 (5) (1962).
[7] A.D. Kodys and E.Y. Choueiri. A critical review of the state of the art in the performance of applied-fiel magnetoplasmadynamic thrusters. 41st AIAA Joint Propulsion Conference, Tucson, Arizona, USA. July 10–13. 2005.
[8] A. Sasoh, Generalized hall acceleration, J. Propul. Power 10 (2) (1994).
[9] M. Tanaka, I. Kimura, Current distribution and plasma acceleration in MPD arcjets with applied magnetic fields, J. Propul. Power 4 (1988).
[10] A. Sasoh, Y. Arakawa, Thrust formula for an applied-field MPD thruster derived from energy conservation equation, J. Propul. Power 11 (1995) 351–356.
[11] R.J. Goldston, P.H. Rutherford, Introduction to Plasma Physics, IOP Publishing Ltd., 1995.
[12] A.V. Arefiev, C.B. Carpenter, Magnetohydrodynamic scenario of plasma detachment in a magnetic nozzle, Phys. Plasmas 12 (2005).
[13] J. Little and E.Y. Choueiri. Divergence of a propulsive plasma flow expanding through a magnetic nozzle. 31st International Electric Propulsion Conference,University of Michigan, Ann Arbor, Michigan, USA, September 20–24. 2009.
[14] R. Myers, Geometric scaling of applied-field magnetoplasmadynamic thrusters, J. Propul. Power 11 (2) (1995).
[15] H. Tahara, Y. Kagaya, T. Yoshikawa, Performance and acceleration process of quasisteady magnetoplasmadynamic arcjets with applied magnetic fields, J. Propul. Power 13 (5) (1997).
[16] I. Kimura and Y. Kagaya. Effect of applied magnetic fields on physical process in an mpd arcjet. AIAA Paper 70–1148 15[5] 1977.
[17] V.B. Tikhonov, S.A. Semenihin, J.R. Brophy, and J. Polk. The experimental performance of the 100 kW lithium MPD thruster with external magnetic field. 24th International ElectricPropulsion Conference [IEPC-95–105]. 1995.
[18] V.B. Tikhonov, S.A. Semenihin, J.R. Brophy, and J. Polk. Performance of 130 kw MPD thruster with an external magnetic field and Li as propellant. 25th International Electric Propulsion Conference [IEPC-97–117]. 1997.
[19] F.Paganucci, P.Rossetti, M.Andrenucci, V.B.Tikhonov, and V.B.Tikhonov. Performance of an Applied Field MPD Thruster. 27th International Electric Propulsion Conference [IEPC-01–132]. 2001.